EMFi-Based Ultrasonic Sensory Array for 3D Localization of Reflectors Using Positioning Algorithms

Ana Jiménez Martín, Álvaro Hernández Alonso, *Member, IEEE*, Daniel Ruíz, Isaac Gude, Carlos De Marziani, María Carmen Pérez, *Member, IEEE*, Fernando J. Álvarez, César Gutiérrez, and Jesús Ureña, *Member, IEEE*

***Abstract*— This paper describes a first prototype of an airborne ultrasonic array that combines pulse-compression techniques with positioning algorithms in order to achieve accurate determination of the position of the reflectors placed in front of the array. The new sensory system is based on an array with four independently controlled emitters and a receiver. The emitters are made of ferroelectrets as active material, leveraging their features to produce broadband air-coupled ultrasonic transducers at low cost. The ultrasonic emissions are encoded with an orthogonal Kasami sequence for each transducer, making possible to transmit simultaneously from each one. Furthermore, one of the main novelties of the proposal is that reflectors are located by means of a spherical trilateration algorithm that uses the time-of-flight of the ultrasonic signals from each transmitter to the receiver, bounced back by the reflector.**

***Index Terms*— Ultrasonic sensory array, EMFi, encoding techniques, 3D localization.**

I. Introduction

THE use of ultrasound for indoor positioning systems is a widely employed solution to obtain high accuracy positions at low cost [1]–[3]. In addition, sonar is a popular sensing technique for achieving robot navigation or obstacle avoidance at low cost and with low energy consumption. In basic systems, with a single transducer, it is only possible to measure the range of the reflector lying within the transducer beam [4], [5]. This renders necessary to use transducer arrays to obtain more information from the environment. In this case, it is possible to obtain bearing information to classify simple reflectors by computing times-of-flight (TOF) for the echoes arriving from different emitters and/or receivers [6]–[9]. One solution for transmitting simultaneously from different transducers is to encode the ultrasonic signal, which also makes possible to obtain higher precision measurements [8], [9]. Furthermore, there are other systems which estimate position from a spectral analysis of the signal [10].

Nevertheless, not only ultrasonic systems have been used for obstacle detection in robotics applications, but also other sensory technologies such as infrared or computer vision. In the case of computer vision, many previous studies have addressed the detection and avoidance of reflectors, using several successful approaches although these have often been characterized by high computational load [11]–[15]. Meanwhile, infrared-based systems have also been developed, but with some significant drawbacks: the range achieved is usually smaller if the aim is to keep the cost low; also, although the detection of the presence of an obstacle is feasible, the determination of an accurate distance can become a complex issue [16]–[20].

In communications and active sensory systems, Code Division Multiple Access (CDMA) techniques are often used to solve multiuser issues [8], [21], [22]. This method assigns a different pseudo-orthogonal code to each user, element or beacon as an identifier, making possible to determine the time of arrival by means of a correlation process between the received signal and the emitted code. Encoded transmissions require a larger bandwidth, thus limiting the kind of transducers that can be considered [23].

Currently available airborne transducers present significant constraints as regards transmitting an encoded ultrasonic signal due to their narrow bandwidth. Furthermore, if a distance range of around one meter in the air is required (as in the case of obstacle localization), the number of suitable transducers is even smaller. One of the most recent alternatives is ferroelectret technology [23]–[25], the subject of the present study. Specifically, we selected a cellular propylene film permanently polarized with quasi-piezoelectric properties and characterized by a low acoustic impedance [26]. One of the

Manuscript received July 24, 2014; revised November 10, 2014; accepted December 13, 2014. Date of publication December 22, 2014; date of current version April 1, 2015. This work was supported in part by the Ministry of Economy and Competitiveness (LORIS Project, ref. TIN2012-38080-C04-01, and DISSECT-SOC project, ref. TEC2012-38058-C03-03), and in part by the University of Alcala (cEYE Project, ref.CCG2013/EXP-043). The associate editor coordinating the review of this paper and approving it for publication was Prof. Zeynep Celik-Butler.

A. Jiménez Martín, Á. Hernández Alonso, D. Ruíz, I. Gude, M. C. Pérez, C. Gutiérrez, and J. Ureña are with the Department of Electronics, University of Alcalá, Alcalá de Henares 28806, Spain (e-mail: ana.jimenez@uah.es; alvaro@depeca.uah.es; daniel.ruiz@depeca.uah.es; isaac.gude@depeca.uah.es; carmen@depeca.uah.es; cesar.gutierrez@depeca.uah.es; urena@depeca.uah.es).

C. De Marziani is with the Department of Electronics, National University of Patagonia San Juan Bosco, Comodoro Rivadavia 9005, Argentina (e-mail: marziani@unpata.edu.ar).

F. J. Álvarez is with the Department of Electrical Engineering, Electronics and Automatics, University of Extremadura, Badajoz 06071, Spain (e-mail: fafranco@unex.es).

Digital Object Identifier 10.1109/JSEN.2014.2384197

main advantages provided by this material is its high mechanical flexibility, which renders the manufacturing process of an array easier, simpler and less expensive. It also presents a broadband frequency response [23], [25] that permits the application of CDMA-based signal processing techniques. This high bandwidth is achieved well below its maximum response at 325kHz [25]. Nevertheless, the efficiency obtained is sufficient to work in air at frequencies around 100kHz.

In robotics and obstacle localization applications, TOFs or DTOFs (Differences in Times-Of-Flight) are often used to estimate bearing information, as well as the position of reflectors in front of an array. With regard to ultrasonic sensory arrays, two different approaches can be considered: on one hand, the array elements have synchronized delays to achieve beamforming [27]; on the other hand, beamforming is not carried out and the only advantage is the common scanning area overlapped by a certain number of transducers. For this second approach, most previous studies have based the estimation of the reflector position on geometrical considerations existing between the transducers and the reflector, determined by the measured TOFs [7], [8], [28]–[30]. Other authors have proposed alternative positioning algorithms, for example PCA (Principal Component Analysis) [9], or biomimetic approach [10], [31]. The solution proposed in the present study consists of applying positioning algorithms, widely used in Local Positioning Systems (LPS), to estimate the position of reflectors.

The application of a positioning algorithm to estimate reflector position has received scant attention in previous studies, and it is often considered together with other geometrical issues [32]. Indeed, ultrasonic systems have already been applied to the development of LPS [1], [3], [33]–[35]. In some of these cases, the ultrasonic beacons were placed in the environment, so that a receiver inside the coverage area could compute its own position by determining the times-of-arrival (TOA) or the differences in times-of-arrival (DTOA) for the emissions from the beacons [2], [36]. The positioning equations obtained from the TOA or DTOA are not linear, so several mathematical techniques can be applied to solve them. According to [37], these techniques can be classified as: geometrical methods, that linearize the location equations [38]; minimization of a cost function, where iterative methods are used to determine the minimum of a cost function, often using Gauss-Newton or Levenberg-Marquardt methods [39]; and Bayesian approaches, where the position of the receiver at a given time t is modeled as a probability function based on the previously obtained measurements [40]. One of the most well-known of these is the resolution of spherical trilateration by means of the Gauss-Newton algorithm [41]. On the other hand, the algorithm based on the bi-determinant described by Cayley-Menger [42] provides a similar accuracy compared to the Gauss-Newton method, but reduces the computational load.

This paper describes the design, manufacture and characterization of an ultrasonic sensory system, capable of estimating the position of a reflector in front of it. The ultrasonic signal processing is based on CDMA techniques, so simultaneous emissions can be made from the emitters.

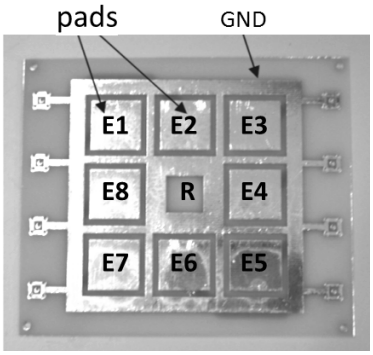

Fig. 1. Printed Circuit Board (PCB) for the sensory system prototype with eight emitters (E_i) and one receiver (R) in the center.

After determining the times-of-flight of ultrasounds from each emitter to the receiver, bounced back by a reflector, these TOFs are used to estimate the reflector position by applying a spherical trilateration algorithm. A first prototype has been developed with multiple transmitters made of EMFi material. Future works will deal with a more complex multi-emitter and multi-receiver system, where inconsistencies about reflector classification in specular environments can be solved and, even, phased array strategies can be applied to electronically guide the emission beam. The manuscript is organized as follows: Section II describes the proposed ultrasonic signal processing, as well as the sensory array manufacturing procedure and the array characterization results, including element sensitivity distribution and crosstalk measurement; Section III deals with the positioning algorithm proposed for the reception stage; Section IV presents some experimental results; and, finally, some conclusions are discussed in Section V.

II. Proposed Sensory System

Due to the limited amount of information obtained from a single ultrasonic transducer, it is common to use sensory arrays in ultrasonic sensory systems. The geometry of the array depends on the application, on the features of the transducers, and on if they work as emitters, as receivers, or both [6], [8], [9]. The array geometry proposed consists of eight square elements arranged in a larger square, as shown in Fig. 1, so that each one can operate as an independent emitter. The eight transducers are positioned so as to achieve maximum symmetry in order to increase the system's capacity to extract information from the scene. The receiver, a commercial microphone (1/4 inch free-field by Bruel and Kjaer [43]), is placed at the center of the array. In order to perform simultaneous emission with the different emitters, the ultrasonic signal is encoded by assigning a specific code to each element as an identifier.

A. Ultrasonic Signal Encoding

The ultrasonic emission is based on encoding the transmission using a Kasami code c_i with a length $L = 255$ bits. These codes are Pseudo-Noise (PN) sequences, and are generated by using linear-feedback shift-registers (LFSR) [44]. A Kasami sequence $c_i[n]$, with values $\{-1, +1\}$, can be

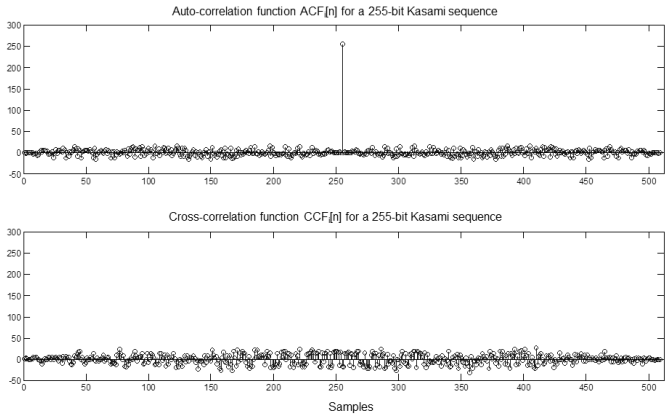

Fig. 2. Auto- and cross-correlation functions, $ACF_i[n]$ and $CCF_i[n]$, for a 255-bit Kasami sequence c_i.

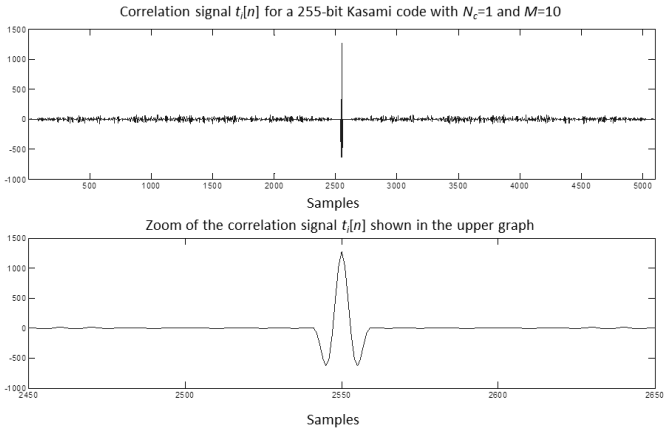

Fig. 3. Example of a correlation signal $t_i[n]$ for a 255-bit Kasami sequence, BPSK modulated with $M = 10$ and $N_c = 1$, and non-coherent detection.

obtained from a maximal sequence and the decimated and concatenated version of this sequence is obtained by performing the module-2 sum of the former with any delayed version of the latter, as can be observed in (1).

$$c_i = m_1 \oplus D^l m_2 \quad \text{for } l < L \tag{1}$$

Where m_1 is a maximal sequence of length $L = 2^{N-1}$ and N is the even number of bits of the LFSR used to generate the Kasami code; m_2 is the sequence obtained from the decimation of m_1 by a factor $q = 2^{N/2} + 1$ and the q-times concatenation of the result; $\oplus$ represents the module-2 sum; and $D^l m_2$ is the sequence obtained by cyclically shifting the m_2 sequence l positions cyclically.

These codes present suitable features for the auto-correlation function (ACF), with high maximum values and reduced sidelobes. With regard to the cross-correlation function (CCF) between orthogonal codes, the values obtained are also reduced, as can be observed in (2) where N is still the number of bits of the LFSR. It is important to note that, for a sequence length $L = 255$ bits, it is possible to have up to 16 orthogonal sequences to achieve simultaneous emissions from different sources [45], [46].

$$ACF_i[n] = \begin{cases} L & n = 0 \\ -1, -2^{N/2} - 1, 2^{N/2} - 1 & n \neq 0 \end{cases}$$
$$CCF_i[n] = -1, -2^{N/2} - 1, 2^{N/2} - 1 \tag{2}$$

Fig. 2 shows the auto- and cross-correlation functions, $ACF_i[n]$ and $CCF_i[n]$, for a Kasami sequence c_i with a length $L = 255$ bits. It is possible to observe how the auto-correlation $ACF_i[n]$ is almost a delta function, whereas the cross-correlation $CCF_i[n]$ presents negligible values compared to the maximum auto-correlation peak.

The encoded emission is adapted to a determined bandwidth by means of a BPSK (Binary Phase Shift Keying) modulation scheme, where the sequence c_i to be emitted is modulated by a period of the carrier signal $s[n]$. After this processing, the final signal $e_i[n]$ emitted by a transducer i is (3):

$$e_i[n] = \sum_{k=0}^{L-1} c_i[k] \cdot s[n - k \cdot M \cdot N_c] \tag{3}$$

Where $c_i[n]$ is the Kasami code to be emitted; $s[n]$ is the symbol of the modulation, formed by $N_c = 1$ periods of the carrier; M is the oversampling of the system, depending on the sampling frequency f_S and on the carrier frequency f_c, so $M = f_S/f_c = 625kHz/62.5kHz = 10$; and L is the length of the Kasami code.

BPSK modulation implies a reduction in the performance of the Kasami sequences, since higher sidelobes appear in the auto- and cross-correlation functions in a non-coherent detection. Nevertheless, the modulation is necessary to focus the emitted energy on the available bandwidth, and the BPSK scheme, with a lower computational load, has been widely used for transmission of ultrasounds in air [6], [7], [21], compared to other schemes already mentioned in [47].

With regard to the reception stage, there is an initial common block dedicated to demodulation of the signal $r[n]$ received by the microphone, implemented through a correlation with a period of the carrier signal $s[n]$, according to (4).

$$d[n] = \sum_{k=0}^{M \cdot N_c - 1} r[k + n] \cdot s[k] \tag{4}$$

Where $d[n]$ is the output from the demodulation stage; $r[n]$ is the input signal coming from the acquisition stage; and $s[n]$ is again the symbol of the demodulation, formed by N_c periods of the carrier, each one represented by M samples. Afterwards, the demodulated signal $d[n]$ should be correlated with every Kasami code c_i emitted by the transducers, so that a final correlation signal $t_i[n]$ can be obtained (5). Fig. 3 shows the correlation signal $t_i[n]$ for a Kasami code c_i with a length $L = 255$ bits, where the code c_i has been BPSK modulated with $M = 10$ and $N_c = 1$.

$$t_i[n] = \sum_{k=0}^{L-1} d[k \cdot (M \cdot N_c) + n] \cdot c_i[k] \tag{5}$$

Where $t_i[n]$ is the correlation output for the code c_i; $d[n]$ is the corresponding demodulation output; $c_i[n]$ is the Kasami code emitted by the transducer i; and L is still the length of the mentioned code.

Lastly, a local maximum detector identifies the maximum values in the correlation signal $t_i[n]$ as correct transmissions in the binary signal $p_i[n]$, by comparing the signal $t_i[n]$ with an experimentally determined threshold U, inside an analysis window W. The non-null values in $p_i[n]$ are used to determine the times-of-flight (TOF) for the corresponding emissions $e_i[n]$. In order to avoid validating wrong peaks in the received correlation signals $t_i[n]$, the analysis is performed in a window W from a distance of 30cm to 125cm from the sensory array. The first limit at 30cm tries to avoid the radio-electrical coupling from the emission. The second one has been estimated to discard echoes from reflections in further and non interesting reflectors existing in the environment. Therefore the local maximum detector is performed in two stages. The first one is to find the highest correlation value over the threshold U, for any of the four correlation signals $t_i[n]$ from the four emitters E_i in the array, in the window W from 30cm to 125cm. This maximum correlation value is considered as a reference for the second phase, where the other peaks from the other correlation functions $t_i[n]$ are sought in the range of 3.4cm around the highest maximum correlation value previously determined; this interval is actually slightly longer than the maximum theoretical difference in times-of-flight between two emitters in the array.

B. Sensory Array Manufacturing

Localization applications using encoded ultrasonic signals require transducers with high sensitivity and a large bandwidth in order to avoid distortion of the encoded signal at ultrasonic frequencies in the range from 20kHz to 90kHz. It is also desirable to have small transducers, as well as ones that can be easily integrated to form the array. To the best of our knowledge, no currently available commercial transducers incorporate these features, so they were manufactured from a commercial electromechanical film (EMFi) by Emfit Ltd [26], [48]. EMFi foil is based on a piezo-polymer material which is characterized by its reduced thickness (typically about $65-70\mu$m), making handling easy; by a very low acoustic impedance (<0.1MRayl), comparable to air; and by a large usable frequency range (from 20kHz to 300kHz). The electromechanical sheet is only metalized on one size, so the rear electrode was defined on a printed circuit board (PCB) where the EMFi active layer was stuck to obtain the transducer.

Thus, the array was manufactured on a PCB, where the eight square elements were defined as pads (see Fig. 1). The active emitting elements were made of EMFi film, with only one foil. They always operated in thickness mode, without any influence from the pad geometry. Their manufacture did not require any special method and consisted of a few simple steps. The size and shape of the elements were defined by the PCB pad, thus the EMFi foil was cut to the desired shape and size and then pasted onto them. To this end, a commercial double-faced adhesive tape was used, which was electrically conductive only through its thickness. The rear of the film, without metallization, was glued onto the substrate side of the PCB, whereas the aluminum side behaved as the upper electrode. Lastly, the upper electrode was connected to the ground plane with silver ink. The resulting prototype is shown in Fig. 4.

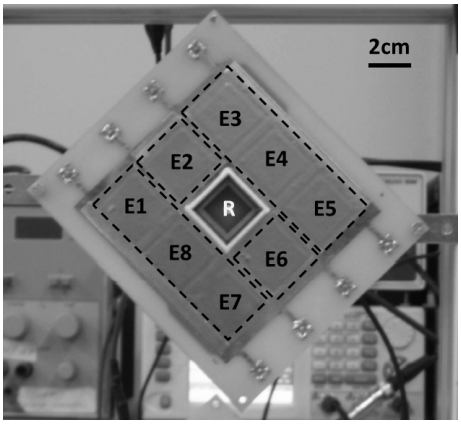

Fig. 4. Array prototype. Dotted lines highlight the pieces of EMFi used to obtain the different emitters E_i. The receiver R in the center is surrounded by a shield (white square).

The intensity of the ultrasonic signal emitted by EMFi, biased with a given voltage, is proportional to the emitting area. Consequently, the larger the element size, the higher the acoustic intensity and, it is therefore, possible to achieve longer distances. Another way to increase the range would be to increase the polarization voltage. Nevertheless, one of the main drawbacks of EMFi is that it requires a high polarization voltage [25], so due to technical reasons concerning our equipment, the driving voltage was limited, and it did not exceed 270Vpp (with no offset). It is important to note that beamforming is not required, so the size ratio between elements is not so critical. Therefore, in this case, a trade-off is reached between the size of the transducer and the distance to be achieved. Previous experiences with transducers based on EMFi suggested that a 2×2cm area would be suitable for exploring distances up to 1m. Thus, the emitters were defined as 2×2cm squares with a nominal separation between centers of successive elements of 28mm, and a gap between elements of 8mm (see Fig. 1). Hence, the global size of the array is 11×13cm. Two different arrays were manufactured to check reproducibility. To simplify the manufacturing process, the maximum number of elements was covered with the same piece of EMFi foil. As can be seen in Fig. 4, in this case three consecutive elements were made with the same piece of film (dashed lines in the image), thus minimizing the number of isolated EMFi squares in the array and reducing a possible border effect. The center position was shielded to mitigate the effects of direct radiation emitted by the elements towards the microphone. This shield, shown in Fig. 4 surrounding the microphone (white square), consisted of the same composite used for the PCB.

C. Array Characterization

The radiation pattern of the square elements in the array is similar to the well-known circular piston source. The main differences are that the square-element pattern is not symmetrical and the sidelobes in one of the directions are higher than those in a circular piston. More specifically,

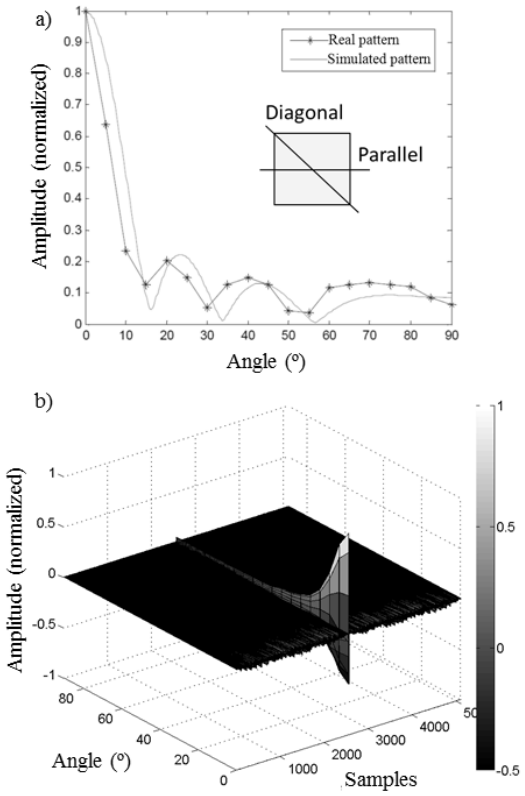

Fig. 5. a) Simulated and experimental radiation pattern for one element of the array in the parallel plane emitting a sinusoidal signal at 62.5kHz. b) Simulated radiation pattern for one element of the array emitting a 255-bit Kasami code at 62.5kHz, showing the ACF as a function of the angle.

the simulated radiation pattern of a square element shows how the pattern in the plane parallel to one side has higher sidelobes than in the diagonal plane. In fact, the intensity of sidelobes in the diagonal plane never exceeded that of the main lobe by more than 5%, whereas in the parallel one it reached up to 20%. For this reason, the microphone, located at the center of the array, received much less energy directly from the emitters in the diagonal than from those located in the horizontal or vertical plane. Therefore, despite having eight emitters in the array, only the four in the diagonal of the receiver are used in this study (Fig. 4: emitters E_1, E_3, E_5 and E_7). Although the radiation pattern is different depending on the plane, the main lobe is similar in both directions, maintaining the symmetry. It was experimentally verified that at 62.5kHz, for example, the global aperture angle was 20.3° in the diagonal and 19.5° in the parallel plane (obtained at −6dB level). The global angle decreased as the frequency increased, achieving 30.6° at 41.7kHz and 15.1° at 83.3kHz, as expected.

To validate the simulation results, the radiation pattern was experimentally obtained by scanning from 0° to 90° in steps of 5°. To this end, the microphone was placed in front of the array at the considered angles, in such a way that the pattern could be obtained independently of the reflector in the environment. Only one transducer in the array was used in each case, and this was excited with a sinusoidal signal at a frequency of 41.7kHz in a first test, and at 62.5kHz in a second one. The theoretical and experimental results for both signals were similar. As an example, Fig. 5.a) shows the results at 62.5kHz in the parallel plane, which presents the largest deviation between the theoretical model and the experimental measurements; note that even in this case the results are satisfactory. In order to analyze the effect of emitter filtering, Fig. 5.b) shows the auto-correlation function according to the angle, plotting one ACF per row, for an element emitting a 255-bit Kasami code at 62.5kHz. It is possible to observe how the maximum auto-correlation value decreases as the angle increases, although the effect of the zeroes in the radiation pattern of an element is masked by the background correlation noise.

To characterize the array, the microphone was again located in front of the array. The individual response of each element was analysed by means of the encoded signal used in the localization application, in order to check the transducer response when it was excited with broadband signals. Therefore, each element emitted a 255-bit Kasami code at different frequencies (41.7kHz, 50kHz, 62.5kHz, 71.4kHz and 83.8kHz). The encoded ultrasonic emission was adapted to the central frequency through a BPSK modulation. The response was evaluated by comparing the maximum values from the auto-correlation function between the received echo and the emitted code. Each figure represents the average of 100 measurements.

The emission from each array element was characterized, firstly checking that each emission was independent of the others, even though only one piece of EMFi had been used in the manufacturing process to cover three consecutive elements in the array (see Fig. 4). To this end, each element was driven by a different Kasami sequence. First, only one element was excited, while the transmission was captured under normal conditions. This test was carried out with the emitting element covered and not covered. By analyzing the auto-correlation functions of both received signals, it was possible to verify that the adjacent elements were not emitting, since no auto-correlation peaks appeared when the emitting element was covered. Second, different elements were excited simultaneously, each one with its corresponding sequence without covering any element. The maximum auto-correlation value for each element was similar to the one in the first test, where only one element was emitting. Therefore, each element could be considered independently, and any possible crosstalk effects could be discarded.

Another issue to consider was the reproducibility of the elements and the homogeneity of the emissions from the different emitters. With regard to the emission from each element, the maximum auto-correlation amplitudes varied slightly between arrays, and also between elements within the same array. Fig. 6 shows a representative case of the auto-correlation peak amplitude for one of the arrays at 50kHz. The differences between elements manufactured with the same piece of EMFi were lower than 10%. However, these differences increase up to 17% if all the elements in the array were considered, which implies that using the same piece of EMFi for several elements provides a more homogeneous emission. This behaviour was also observed for the other array where the maximum differences rose to 20%. Therefore, the results were similar, not only for both

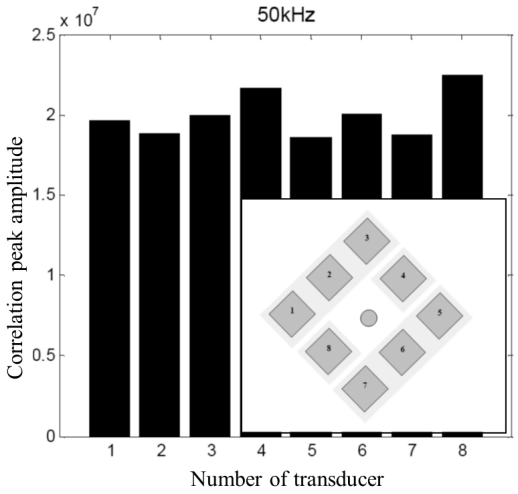

Fig. 6. Maximum auto-correlation amplitudes when emitting a BPSK modulated 255-bit Kasami encoded signal at 50kHz.

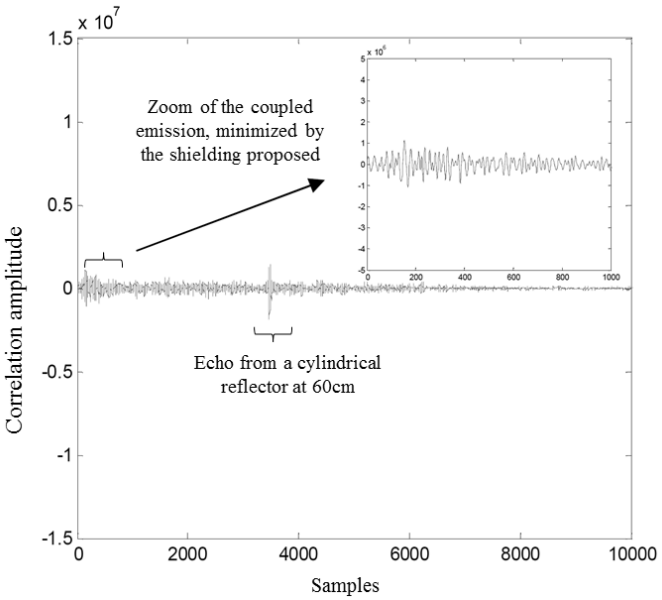

Fig. 7. Correlation function corresponding to the received echo from a cylindrical reflector after the microphone shielding.

arrays, but also for all the analyzed frequencies. Note that these differences increased with frequency, thus obtaining the highest value up to 20% at 83.3kHz. In sum, the use of a single piece of EMFi to manufacture the array, defining the size of each element solely by means of the metal pad, simplifies the manufacturing process and not only achieves an independent response for each element, but also reduces differences in emission, thus providing much more uniform responses. It is important for the auto-correlation function to present a uniform amplitude, independently of the array element, since auto-correlation peaks degrade in noisy environments and/or with weak reflectors (those that do not return back a large amount of energy). In these cases, the sidelobes in correlation functions can achieve the same amplitudes as the main peak, thus rendering difficult to discriminate the echo arrivals and to determine the corresponding times-of-flight. A uniform response yields the same behavior in all the array elements.

The experimental results showed the systematic appearance of an extra peak in the auto-correlation function. This peak may correspond to direct radio-electrical coupling since it was weaker when the diagonal elements were emitting, than when the horizontal and vertical ones were. In order to minimize this adverse effect, only the four elements located in the diagonal of the microphone were used, thereby ensuring that the horizontal and vertical elements did not have a higher direct-coupling signal. Furthermore, the center of the array, where the microphone was located, was shielded. Note that the presence of a coupled signal implies a blind detection zone near the sensory array that increases with the length of the encoded emission. From a theoretical point of view, this blind zone reaches up to 69cm approximately, corresponding to a 255-bit Kasami code at 62.5kHz. Nevertheless, the signal encoding allows the reduction of the blind zone, since the detection of these codes is still feasible, even when large percentages of their length have been lost by overlapping with the coupled emission [49]. In this case, it has been checked that the blind zone can be considered up to 30cm from the array.

The auto-correlation function obtained for the echo from a cylindrical reflector with a diameter of 2.7cm at a distance of 60cm from the array is shown in Fig. 7. It was possible to estimate the position of the reflector from the maximum peaks of the auto-correlation functions, assuming a constant ultrasound speed. Fig. 7 also shows a zoom of the coupling effect, illustrating how this effect becomes minimal after shielding the microphone and using only the elements of the two diagonals (emitters E_1, E_3, E_5 and E_7). It is important to note that the echo received in Fig. 7 was degraded in a realistic environment, compared to the ideal properties of the correlation functions shown in Fig. 3. This deterioration was mainly due to noise from the environment, the cross-correlation interference from several Kasami sequences transmitted simultaneously by each array element (Multiple Access Interference, MAI), the bandwidth constraint and radiation patterns presented by the ultrasonic transducers, and the position (distance and angle) as well as the kind of reflector (size and material).

III. Positioning Algorithm Proposal

The geometry proposed for the array implies that the direct measurement obtained from the TOF is the sum of the distance l_i from the emitter E_i to the reflector P and the distance l between the reflector P and the receiver R. Fig. 8 shows the geometrical scheme for the localization of a point reflector P. Therefore, it is firstly necessary to determine the distance l between the reflector P and receiver R, and, then, to estimate the absolute distance l_i between an emitter E_i and the reflector P, in order to locate the reflector P, by using a spherical algorithm.

The simultaneous emission of an orthogonal Kasami code c_i by each emitter E_i, where $i = \{1, 3, 5, 7\}$, and, afterwards, the reception and correlation, as was explained in Section II-A above, makes possible to measure the times-of-flight TOF_i between the emitter E_i and the receiver R, bounced back from the reflector P. Taking advantage of the array geometry shown

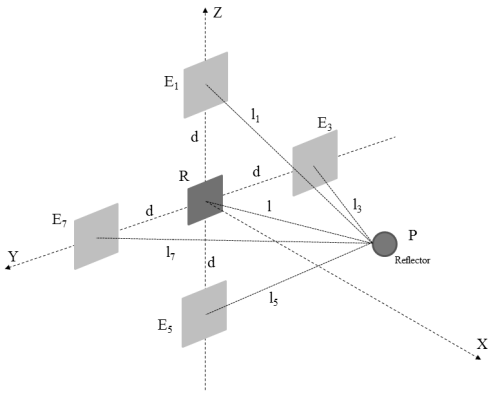

Fig. 8. Geometrical distribution and parameters for a 3D localization.

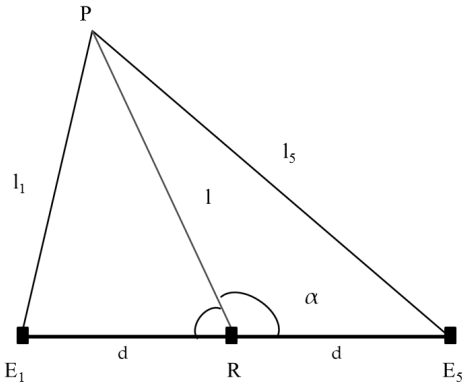

Fig. 9. Geometrical considerations to compute the distance l between the reflector P and the receiver R.

in Fig. 9, it is posible to obtain the distance l, by applying the cosine theorem in the triangles $\overset{\Delta}{PRE_1}$ and $\overset{\Delta}{PRE_5}$:

$$\begin{aligned} {l_1}^2 &= l^2 + d^2 - 2 \cdot l \cdot d \cdot cos(\pi - \alpha) \\ &= l^2 + d^2 + 2 \cdot l \cdot d \cdot cos(\alpha) \end{aligned} \quad (6)$$

$${l_5}^2 = l^2 + d^2 - 2 \cdot l \cdot d \cdot cos(\alpha) \quad (7)$$

Where d is the distance between the receiver R and the emitters E_i, this value is known and is the same for all the emitters E_i; α is the angle formed between the ray reflected by the reflector P and the line created by the emitters $\overline{E_1 E_5}$ (see Fig. 9); and TOF_1 and TOF_5 are the times-of-flight measured for the emissions from E_1 and E_5, respectively.

The angle α is not known, but by, adding equations (6) and (7), it is possible to discard this parameter. Thus, taking into account that $c \cdot TOF_1 = l + l_1$ and $c \cdot TOF_5 = l + l_5$, where c is the ultrasound speed, the distance l is obtained as (8) from the measured times-of-flight TOF_1 and TOF_5 and from the known geometrical parameter d.

$$l = \frac{(c \cdot TOF_1)^2 + (c \cdot TOF_5)^2 - 2 \cdot d^2}{2 \cdot c \cdot TOF_1 + 2 \cdot c \cdot TOF_5} \quad (8)$$

The same process can be performed with the triangles $\overset{\Delta}{PRE_3}$ and $\overset{\Delta}{PRE_7}$ to obtain a second value for the distance l. The final value considered for the distance l between the receiver R and the reflector P can be computed as the mean of the two previous values obtained with the emitters $E_1 - E_5$ and $E_3 - E_7$, respectively. After determining the distance l, it is possible to calculate the distances l_i and to estimate the position of the reflector P by means of a spherical trilateration algorithm.

A spherical algorithm based on the Cayley-Menger bi-determinant is proposed in [42] to compute the position of the reflector P. This positioning algorithm obtains the 3D (three dimensional) position of the reflector, (x, y, z), with regard to the array reference system by using the distances l_i measured between the emitters E_i and the reflector P. The advantage of this method is that it directly provides the position of the reflector, thus reducing the computational load compared with other iterative resolution methods, such as the Gauss-Newton approach [41], [50].

One of the figures of merit that characterize a location system is the Position Dilution Of Precision (PDOP) [51]. The PDOP relates the uncertainty in the reflector position estimation (x, y, z) with the uncertainty in the measurements of distances l_i. This parameter provides a ratio about how errors in the determination of distances l_i affect to errors in the estimation of the reflector position (x, y, z): the less the PDOP is, the less sensitive to errors the approach becomes. The mathematical expression for the PDOP can be observed in (9), where σ_x, σ_y and σ_z are the standard deviations for reflector position estimation and σ is the standard deviation of the distance measurement error.

$$PDOP = \frac{\sqrt{{\sigma_x}^2 + {\sigma_y}^2 + {\sigma_z}^2}}{\sigma} \quad (9)$$

Furthermore, the PDOP parameter is not constant for all the scanned area, but it depends on the reflector position, as well as the array geometry. In this sense, Fig. 10 shows the theoretical PDOP in the plane YZ in front of the sensory array for a reflector P at $x = 40$cm (Fig. 10.a) and $x = 1$m (Fig. 10.b). The four circles at the center in Fig. 10 are the projections of the emitters E_i on the plane YZ. It can be observed how the PDOP varies from 15 to 25 in the plane YZ at $x = 40$cm, and from 35 to 40 at $x = 1$m also in the plane YZ, what implies less precision at further distances. As an example, the errors for distances l_i propagate 15 times greater for the position estimation (x, y, z) at $x = 40$cm in the central scanned region in front of the sensory array.

IV. Experimental Results

For experimental tests in 3D, it was necessary to use a reflector P that behaved as a point, so that all the echoes would come from the same point. The considered reflector P was a cylindrical pole with a diameter $D = 2.3$cm wrapped with aluminum foil. This reflector was placed on a metal support 150cm in length, where a guide was used to vertically move the reflector P. In order to avoid echoes coming from the metal support, which was larger than the reflector P, some pads were attached to absorb the acoustic signal reflected onto it. Thus, the echo only came from the reflector P. In all

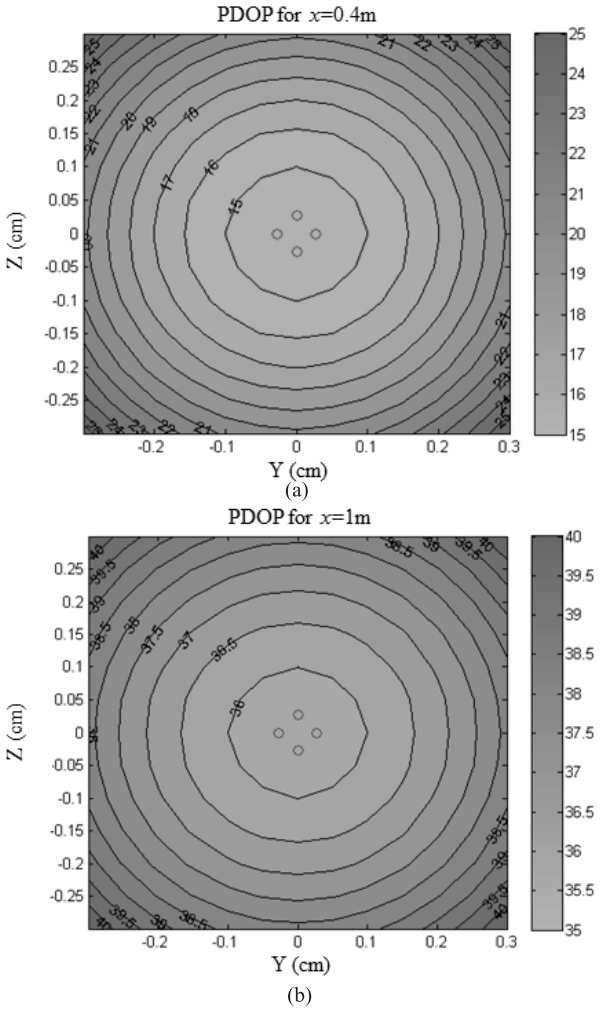

Fig. 10. Theoretical PDOP values in the plane YZ for a reflector P: (a) at $x = 40$cm and (b) $x = 1$m from the sensory array.

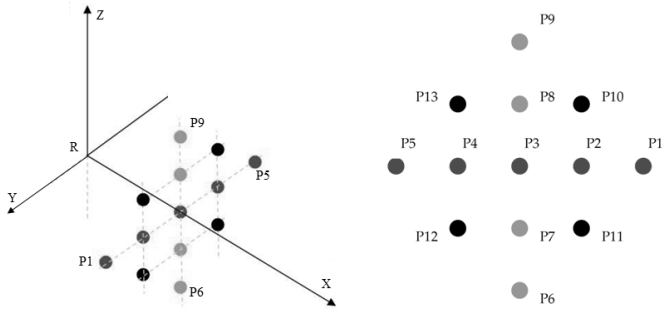

Fig. 11. Pattern of positions Pn considered in the experimental tests.

the experimental tests, since only the first echo to arrive was taken into account for localization and the successive emission firings were sufficiently delayed, multipath issues were not considered. Even if any additional reflection occurs within the length of the transmitted signal, the first echo corresponding to the direct line-of-sight can be identified thanks to the correlation properties of Kasami codes.

The positions Pn, with $n = \{1, 2, \ldots 13\}$, shown in Fig. 11 were considered for measurements acquisition, placed at different distances x of 40cm, 60cm, 80cm and 100cm, all of them in a plane with $x = K$. For each distance x,

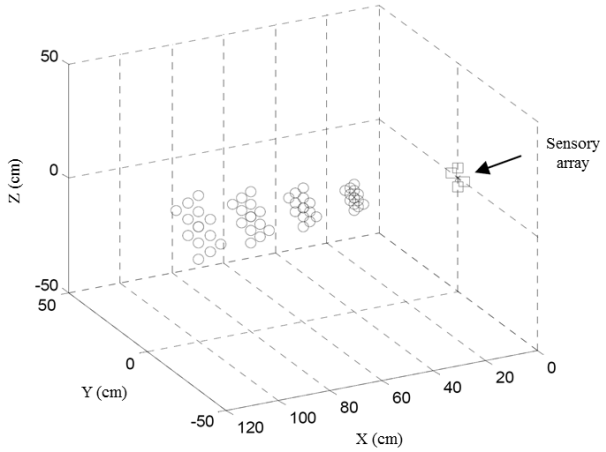

Fig. 12. Theoretical positions Pn where the reflector has been placed.

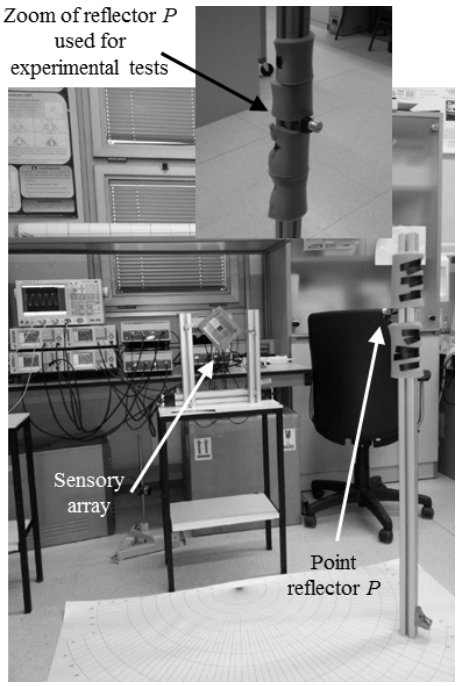

Fig. 13. Experimental setup used for measurements in positions Pn, with a zoom of the point reflector P.

the reflector was placed at the points Pn described in Fig. 11, according to the following pattern: five points $P0 - P5$ in the horizontal axis (plane $z = 0$); four points $P6 - P9$ in the vertical axis (plane $y = 0$); and, lastly, another four points $P10 - P13$ in diagonal. The angle formed by the segment $R - P1$ (from the receiver R to the point $P1$) and the segment $R - P3$ (from the receiver R to the point $P3$) was 8°, whereas the angle between the segment $R - P2$ and $R - P3$ was 4°. Furthermore, the point $P3$ was always placed in the axial axis of the sensory array. The other positions can be obtained by taking into account the geometrical distribution of the pattern. For every considered distance x, these angular values were kept constant, so that the separation between the measurement points Pn tended to increase. Fig. 12 shows the 52 theoretical points Pn where the reflector P was placed, whereas Fig. 13 depicts the experimental setup for these tests

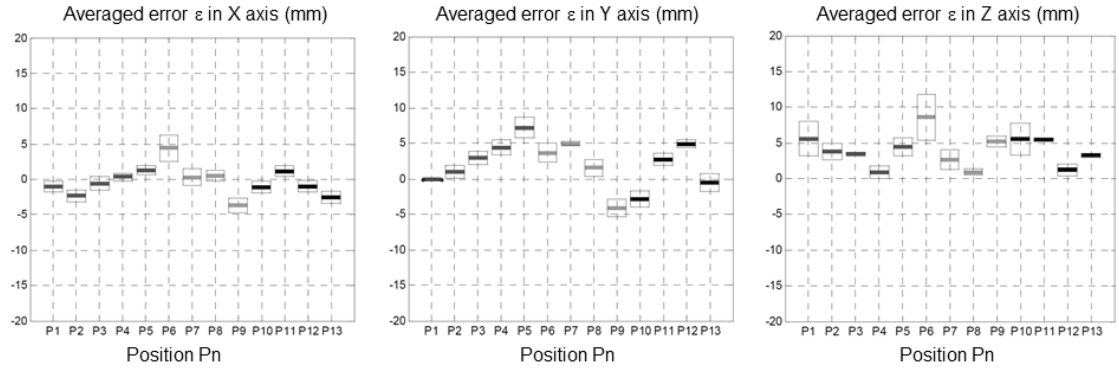

Fig. 14. Averaged errors ε and standard deviations σ for a distance $l = 40$cm.

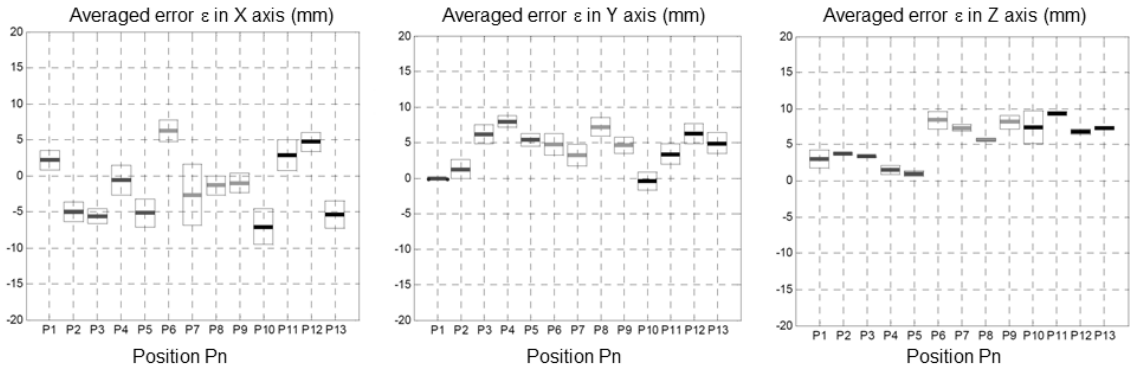

Fig. 15. Averaged errors ε and standard deviations σ for a distance $l = 60$cm.

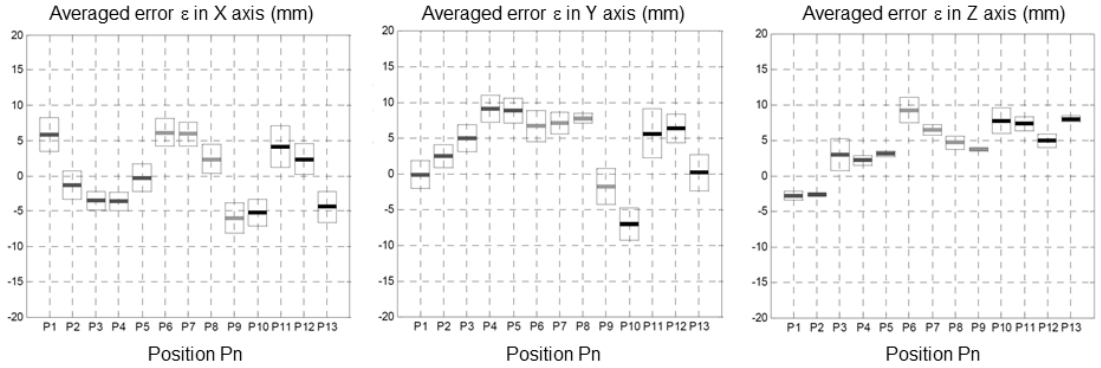

Fig. 16. Averaged errors ε and standard deviations σ for a distance $l = 80$cm.

with a zoom of the point reflector P. The transmitters have been driven by the 9200 power amplifiers and the WW5062 arbitrary waveform generators, both manufactured by Tabor Electronics Ltd. On the other hand, the receiver consists of a microphone model 4939 [43] and a pre-amplifier model 2670 by Brüel & Kjaer, connected to a UltraSoundGate Mic Power Module from Avisoft Bioacoustics e.K., which provides acquired data easily to a PC (Personal Computer) to process them. This experimental setup does not allow any real-time performance, although all the signal processing proposed for signal encoding and TOF detection can be implemented in real-time approaches, as has been already detailed in [2] and [8].

At each position, 100 measurements were acquired, in order to compute the average errors ε and the standard deviations σ. Fig. 14 shows the results obtained for a distance $l = 40$cm, where the averaged errors ε for X and Y axes were around $\pm$5mm, whereas for the Z axis the errors were positive biased, with values from 0 to $+$10mm. This bias was probably due to the difficulty of an accurate placement of the reflector P in front of the sensory array for every point Pn, especially in the Z axis. In fact, similar bias values were obtained for distances $l = 60$cm, 80cm and 100cm, as shown in Figs. 15, 16 and 17, respectively. It can be seen that the bias effect was almost constant in the Z axis. On the other hand, as expected, the average error increased with the distance l between the

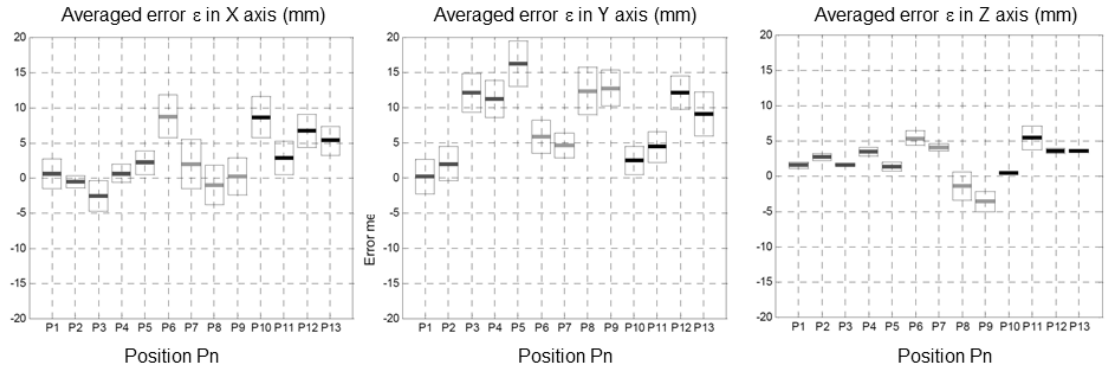

Fig. 17. Averaged errors ε and standard deviations σ for a distance $l = 100$cm.

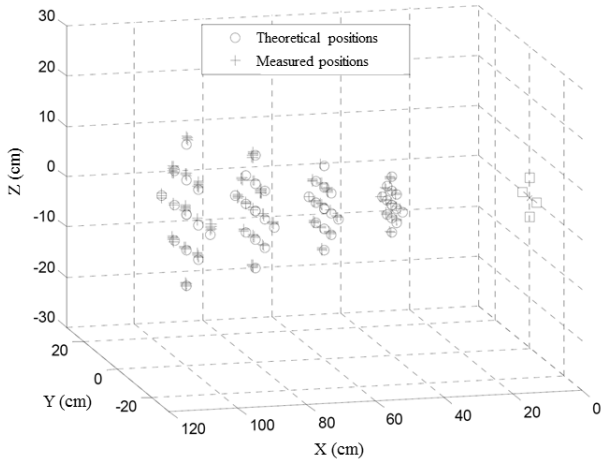

Fig. 18. Theoretical positions and positions measured by the proposed sensory array in the experimental tests.

reflector and receiver, as well as the standard deviation σ. However, despite the bias effect, the resulting errors were in the range of millimeters for all the distances and angles considered. Furthermore, it should be noted that, in order to avoid the effect of outliers, those positioning results with errors ε higher than $1.95 \cdot \sigma$ were discarded. For all the considered cases, the percentage of outliers was below 10%. Note too that no additional noise was involved in the experimental tests, apart from the ordinary noise in the lab.

All the analyzed points are depicted in Fig. 18, together with the theoretical positions. In sum, the proposed sensory array can locate a reflector with averaged errors around $\pm$5mm, increasing up to 10mm in the worst cases. Compared to previous proposals, such as those proposed in [6], [7], and [30] where errors lower than 0.2mm and than 0.2° are obtained with greater ranges using SensComp electrostatic transducers, the approach here presented provides suitable results, taking into account the significant difference in the amount of acoustic energy transmitted by this system and by the others. The customized EmFi emitter (2cm $\times$ 2cm) has a Sound Pressure Level (SPL) of about 75dB re 20μPa at 0.25m [23], whereas the Senscomp electrostatic transducer used in the other proposals has a SPL of 110dB re 20μPa at 1m [52]. This implies that much less acoustic energy is transmitted, and, in spite of that, acceptable results are achieved for most applications of this kind of systems.

V. Conclusion

This paper has proposed a new sensory array prototype based on an electromechanical material for performing 3D localization of reflectors using CDMA techniques. There are two main characteristics to remark. On the one hand, the prototype is based on an array of four emitters made of electromechanical film. The main advantage of using this film as active element in the transducers is that it simplifies the array design, permitting the manufacture of different shapes and sizes at low cost and with the large bandwidth required by CDMA approaches. On the other hand, the applied CDMA techniques enable simultaneous transmission from four transducers in order to obtain more information from the environment with only one emission. This operation is accomplished by means of an algorithm that performs spherical trilateration by using the times-of-flight for the emission from each transducer in the array. This first prototype has achieved the localization of a point-like reflector with an average error lower than 10mm in 3D positioning tests.

References

[1] N. B. Priyantha, A. Chakraborty, and H. Balakrishnan, "The Cricket location-support system," in *Proc. 6th Annu. Int. Conf. Mobile Comput. Netw.*, 2000, pp. 32–43.

[2] J. Ureña *et al.*, "Advanced sensorial system for an acoustic LPS," *Microprocess. Microsyst.*, vol. 31, no. 6, pp. 393–401, 2007.

[3] J. C. Prieto *et al.*, "Performance evaluation of 3D-LOCUS advanced acoustic LPS," *IEEE Trans. Instrum. Meas.*, vol. 58, no. 8, pp. 2385–2395, Aug. 2009.

[4] R. Kuc and M. W. Siegel, "Physically based simulation model for acoustic sensor robot navigation," *IEEE Trans. Pattern Anal. Mach. Intell.*, vol. PAMI-9, no. 6, pp. 766–778, Nov. 1987.

[5] J. J. Leonard and H. F. Durrant-Whyte, "Mobile robot localization by tracking geometric beacons," *IEEE Trans. Robot. Autom.*, vol. 7, no. 3, pp. 376–382, Jun. 1991.

[6] H. Peremans, K. Audenaert, and J. M. Van Campenhout, "A high-resolution sensor based on tri-aural perception," *IEEE Trans. Robot. Autom.*, vol. 9, no. 1, pp. 36–48, Feb. 1993.

[7] L. Kleeman and R. Kuc, "Mobile robot sonar for target localization and classification," *Int. J. Robot. Res.*, vol. 14, no. 4, pp. 295–318, 1995.

[8] A. Hernández *et al.*, "Ultrasonic ranging sensor using simultaneous emissions from different transducers," *IEEE Trans. Ultrason., Ferroelectr., Freq. Control*, vol. 51, no. 12, pp. 1660–1670, Dec. 2004.

[9] J. A. Jiménez *et al.*, "Using PCA in time-of-flight vectors for reflector recognition and 3-D localization," *IEEE Trans. Robot.*, vol. 21, no. 5, pp. 909–924, Oct. 2005.
[10] J. Reijniers and H. Peremans, "Biomimetic sonar system performing spectrum-based localization," *IEEE Trans. Robot.*, vol. 23, no. 6, pp. 1151–1159, Dec. 2007.
[11] A. Ohya, A. Kosaka, and A. Kak, "Vision-based navigation by a mobile robot with obstacle avoidance using single-camera vision and ultrasonic sensing," *IEEE Trans. Robot. Autom.*, vol. 14, no. 6, pp. 969–978, Dec. 1998.
[12] D. Droeschel, D. Holz, J. Stuckle, and S. Behnke, "Using time-of-flight cameras with active gaze control for 3D collision avoidance," in *Proc. IEEE Int. Conf. Robot. Autom. (ICRA)*, May 2010, pp. 4035–4040.
[13] J. Kim and Y. Do, "Moving obstacle avoidance of a mobile robot using a single camera," *Proc. Eng.*, vol. 41, pp. 911–916, Sep. 2012, doi: 10.1016/j.proeng.2012.07.262.
[14] S. Almansa-Valverde, J. C. Castillo, and A. Fernández-Caballero, "Mobile robot map building from time-of-flight camera," *Expert Syst. Appl.*, vol. 9, no. 10, pp. 8835–8843, 2012.
[15] J. Biswas and M. Veloso, "Depth camera based indoor mobile robot localization and navigation," in *Proc. IEEE Int. Conf. Robot. Autom. (ICRA)*, May 2012, pp. 1697–1702.
[16] C. R. Kube, "A minimal infrared obstacle detection scheme," *Robot. Practitioner*, vol. 2, no. 2, pp. 15–20, 1996
[17] P. M. Novotny and N. J. Ferrier, "Using infrared sensors and the Phong illumination model to measure distances," in *Proc. IEEE Int. Conf. Robot. Autom. (ICRA)*, vol. 2, May 1999, pp. 1644–1649.
[18] C. S. Dima, N. Vandapel, and M. Hebert, "Classifier fusion for outdoor obstacle detection," in *Proc. IEEE Int. Conf. Robot. Autom. (ICRA)*, vol. 1, Apr./May 2004, pp. 665–671.
[19] W. Liu and A. F. T. Winfield, "Implementation of an IR approach for autonomous docking in a self-configurable robotics system," in *Proc. Towards Auto. Robot. Syst. (TAROS)*, 2009, pp. 251–258.
[20] G. Lee and N. Y. Chong, "Low-cost dual rotating infrared sensor for mobile robot swarm applications," *IEEE Trans. Ind. Informat.*, vol. 7, no. 2, pp. 277–286, May 2011.
[21] K.-W. Jörg and M. Berg, "Sophisticated mobile robot sonar sensing with pseudo-random codes," *Robot. Auto. Syst.*, vol. 25, nos. 3–4, pp. 241–251, 1998.
[22] J. Ureña, M. Mazo, J. J. García, A. Hernández, and E. Bueno, "Classification of reflectors with an ultrasonic sensor for mobile robot applications," *Robot. Auto. Syst.*, vol. 29, no. 4, pp. 269–279, 1999.
[23] A. Jiménez *et al.*, "EMFi-based ultrasonic transducer for robotics applications," *Sens. Actuators A, Phys.*, vol. 148, no. 1, pp. 342–349, 2008.
[24] M. Paajanen, J. Lekkala, and K. Kirjavainen, "Electromechanical film (EMFi)—A new multipurpose electret material," *Sens. Actuators A, Phys.*, vol. 84, nos. 1–2, pp. 95–102, 2000.
[25] A. Streicher, R. Müller, H. Peremans, and R. Lerch, "Broadband ultrasonic transducer for a artificial bat head," in *Proc. IEEE Symp. Ultrason.*, vol. 2. Honolulu, HI, USA, Oct. 2003, pp. 1364–1367.
[26] K. Kirjavainen, "Electromechanical film and procedure for manufacturing same," U.S. Patent 4 654 546 A, Mar. 31, 1987.
[27] C. Diego, A. Hernández, A. Jiménez, F. J. Álvarez, R. Sanz, and J. Aparicio, "Ultrasonic array for obstacle detection based on CDMA with Kasami codes," *Sensors*, vol. 11, no. 12, pp. 11464–11475, 2011.
[28] M. Yang, S. L. Hill, and J. O. Gray, "Localization of plane reflectors using a wide-beamwidth ultrasound transducer arrangement," *IEEE Trans. Instrum. Meas.*, vol. 46, no. 3, pp. 711–716, Jun. 1997.
[29] D.-W. Jung, Z.-S. Lim, B.-G. Kim, and N.-K. Kim, "Multi-channel ultrasonic sensor system for obstacle detection of the mobile robot," in *Proc. Int. Conf. Control, Autom. Syst. (ICCAS)*, Oct. 2007, pp. 2347–2351.
[30] D. Browne and L. Kleeman, "An advanced sonar ring design with 48 channels of continuous echo processing using matched filters," in *Proc. IEEE/RSJ Int. Conf. Intell. Robots Syst. (IROS)*, Oct. 2009, pp. 4040–4046.
[31] F. Schillebeeckx and H. Peremans, "Biomimetic sonar: 3D-localization of multiple reflectors," in *Proc. IEEE/RSJ Int. Conf. Intell. Robots Syst. (IROS)*, Oct. 2010, pp. 3079–3084.
[32] A. Canclini, F. Antonacci, J. Filos, A. Sarti, and P. Naylor, "Exact localization of planar acoustic reflectors in three-dimensional geometries," in *Proc. Int. Workshop Acoust. Signal Enhancement (IWAENC)*, Sep. 2012, pp. 1–4.
[33] A. Ward, A. Jones, and A. Hopper, "A new location technique for the active office," *IEEE Pers. Commun.*, vol. 4, no. 5, pp. 42–47, Oct. 1997.
[34] C. De Marziani *et al.*, "Acoustic sensor network for relative positioning of nodes," *Sensors*, vol. 9, no. 11, pp. 8490–8507, 2009.
[35] D. Ruiz, E. García, J. Ureña, D. de Diego, D. Gualda, and J. C. García, "Extensive ultrasonic local positioning system for navigating with mobile robots," in *Proc. 10th Workshop Posit., Navigat. Commun. (WPNC)*, Mar. 2013, pp. 1–6.
[36] C. De Marziani *et al.*, "Simultaneous measurement of times-of-flight and communications in acoustic sensor networks," in *Proc. IEEE Int. Workshop Intell. Signal Process.*, Sep. 2005, pp. 122–127.
[37] F. Seco, A. R. Jiménez, C. Prieto, J. Roa, and K. Koutsou, "A survey of mathematical methods for indoor localization," in *Proc. IEEE Int. Symp. Intell. Signal Process. (WISP)*, Aug. 2009, pp. 9–14.
[38] J. J. Caffery, Jr., "A new approach to the geometry of TOA location," in *Proc. 52nd Veh. Technol. Conf. IEEE-VTS Fall VTC*, vol. 4, May 2000, pp. 1943–1949.
[39] S. Mazuelas *et al.*, "Dynamic estimation of optimum path loss model in a RSS positioning system," in *Proc. IEEE/ION Posit., Location Navigat. Symp.*, May 2008, pp. 679–684.
[40] A. D. Koutsou *et al.*, "Preliminary localization results with an RFID based indoor guiding system," in *Proc. IEEE Int. Symp. Intell. Signal Process. (WISP)*, Oct. 2007, pp. 1–6.
[41] J. Yan, C. Tiberius, G. Bellusci, and G. Janssen, "Feasibility of Gauss–Newton method for indoor positioning," in *Proc. IEEE/ION Posit., Location Navigat. Symp.*, Monterey, CA, USA, May 2008, pp. 660–670.
[42] F. Thomas and L. Ros, "Revisiting trilateration for robot localization," *IEEE Trans. Robot.*, vol. 21, no. 1, pp. 93–101, Feb. 2005.
[43] *Condenser Microphone Cartridges—Types 4133 to 4181*, Brüel and Kjær, Nærum, Denmark, 2007.
[44] T. Kasami, "Weight distribution formula for some class of cyclic codes," in *Combinational Mathematics and its Applications*. Chapel Hill, NC, USA: Univ. North Carolina Press, 1969.
[45] D. V. Sarwate and M. B. Pursley, "Crosscorrelation properties of pseudorandom and related sequences," *Proc. IEEE*, vol. 68, no. 5, pp. 593–619, May 1980.
[46] V. A. Kumar, A. Mitra, and S. R. M. Prasana, "On the effectivity of different pseudo-noise and orthogonal sequences for speech encryption from correlation properties," *Int. J. Inf. Technol.*, vol. 4, no. 2, pp. 455–462, 2007.
[47] F. J. Álvarez *et al.*, "A comparative analysis of two modulation schemes for the efficient transmission of complementary sequences in a pulse compression ultrasonic system," in *Proc. IADAT-tcn Int. Conf. Telecommun. Comput. Netw.*, Dec. 2004, pp. 1–5.
[48] *Emfit Film Product Specification*, Emfit Ltd., Austin, TX, USA, 2004.
[49] A. Hernández, J. Ureña, M. Mazo, J. J. García, A. Jiménez, and F. J. Álvarez, "Reduction of blind zone in ultrasonic transmitter/receiver transducers," *Sens. Actuators A, Phys.*, vol. 133, no. 1, pp. 96–103, 2007.
[50] D. Ruiz *et al.*, "Hyperbolic ultrasonic LPS using a Cayley–Menger bideterminant-based algorithm," in *Proc. IEEE Instrum. Meas. Technol. Conf. (I2MTC)*, Singapore, May 2009, pp. 785–790.
[51] G. Taraldsen, "Dilution of precision in acoustics," in *Proc. 34th Scandin. Symp. Phys. Acoust.*, Jan. 2011.
[52] *Series 600 Open Face Electrostatic Ultrasonic Sensor*, Senscomp, Inc., Livonia, MI, USA, 2004.

Ana Jiménez Martín received the Degree in physics from the Complutense University of Madrid, Madrid, Spain, and the Ph.D. degree in material engineering from the Polytechnic University of Madrid, Madrid, in 2003. She has worked in MBE growth, fabrication, and characterization of GaN heterostructures for electronic applications. She joined the Department of Electrical Engineering, University of Alcalá, Madrid, in 2004, as an Assistant Professor. Her research interests are focused on ultrasonic transducers and underwater acoustics.

Álvaro Hernández Alonso received the Ph.D. degree from the University of Alcalá (UAH), Madrid, Spain, and Blaise Pascal University, Clermont-Ferrand, France, in 2003. He is currently an Associate Professor of Digital Systems and Electronic Design with the Department of Electronics, UAH. His research areas are in multisensor integration, electronic systems for mobile robots, and digital and embedded systems.

Daniel Ruíz received the B.S. degree in telecommunication engineering, the M.Sc. degree in advanced electronics systems, and the Ph.D. degree in electronics from the University of Alcalá, Madrid, Spain, in 2006, 2009, and 2011 respectively. Since 2006, he has collaborated on several research projects in the areas of local positioning systems, signal processing, and multisensor integration.

Isaac Gude received the B.S. degree in industrial technical engineering and electronics engineering from the University of Alcalá, Madrid, Spain, in 2007 and 2010, respectively, where he has been focused on the study and development of ultrasonic transducer arrays for local positioning systems, mainly for mobile robots applications, as a Researcher with the Department of Electronics.

Carlos De Marziani received the Electronics Engineering degree from the National University of Patagonia San Juan Bosco, Comodoro Rivadavia, Argentina, in 2001, and the Ph.D. degree from the Department of Electronics, University of Alcalá, Madrid, Spain, in 2007. He is currently a Professor of Digital Systems with the Department of Electronics, National University of Patagonia San Juan Bosco, and also an Adjunct Researcher with the National Council on Scientific and Technical Research, Argentina. His research areas are in sensor networks, multisensor integration, electronic systems for mobile robots, and digital signal processing for underwater applications.

María Carmen Pérez (M'07) received the M.S. degree in electronics engineering and the Ph.D. degree from the University of Alcalá, Madrid, Spain, in 2004 and 2009, respectively, where she is currently an Assistant Professor with the Department of Electronics. Since 2003, she has collaborated on several research projects in the areas of sequence design, low-level ultrasonic signal processing, and computing architectures.

Fernando J. Álvarez received the Physics degree from the University of Sevilla, Seville, Spain, the Electronics Engineering degree from the University of Extremadura, Badajoz, Spain, and the Ph.D. degree in electronics from the University of Alcalá, Madrid, Spain, in 2006. He is currently an Associate Professor of Digital Electronics with the Department of Electrical Engineering, Electronics and Automation, University of Extremadura, where he is also the Head of the Sensory Systems Group. His research areas of interest include local positioning systems, ultrasonic signal processing, and embedded computing.

César Gutiérrez was born in Cantabria, Spain, in 1987. He received the bachelor's degree in industrial technical engineering with a specialization in industrial electronics from the Technical Engineering School of Bilbao, Bilbao, Spain, in 2011, and the master's degree in advanced electronic systems and intelligent systems from the University of Alcalá, Madrid, Spain, in 2013, where he is currently pursuing the Ph.D. degree at the Department of Electronics. His research interests include ultrasonic imaging, ultrasonic arrays, digital signal processing, and parallel programming with GPUs.

Jesús Ureña received the B.S. degree in electronics engineering and the M.S. degree in telecommunications engineering from the Polytechnical University of Madrid, Madrid, Spain, in 1986 and 1992, respectively, and the Ph.D. degree in telecommunications from the University of Alcalá, Madrid, in 1998, where he has been with the Department of Electronics, since 1986, and currently as a Professor. From 1993 to 1997, he was the Head of the Department of Electronics. He has collaborated in several educational and research projects in the area of electronic control and sensory systems for mobile robots and wheelchairs, and electronic distributed systems for railways. His current research interests are in the areas of low-level ultrasonic signal processing, local positioning systems, and sensory systems for railway infrastructure.